

# Overcoming the Intrinsic Limitations of Fast Charging Lithium-Ion Batteries Using Integrated Acoustic Streaming

An Huang, Haodong Liu, Ping Liu,\* and James Friend\*

A lithium-ion battery's maximum charge rate and energy density are intrinsically limited by the ion diffusion rate in the electrolyte. Most research focuses on materials science solutions to this problem, with gradual improvement over the years. A mechanical solution is proposed to integrate an MHz-order frequency surface acoustic wave (SAW) device into an existing 1.8 Ah multilayered Li-ion pouch cell to enhance the ion diffusion rate and the overall battery performance. Both the charging rate and cycling lifetime are improved from SAW. At a 6C (10 min) charge and C/3 discharge rate, typical of electric vehicle applications, integrating SAW into the Li-ion cell doubles the energy density and maintains at least 72% of the battery's initial capacity after 2000 cycles. Moreover, using SAW quantifiably reduces battery degradation in these conditions as determined by optical imaging, scanning electron microscopy, X-ray diffraction, and neutron diffraction. The use of SAW appears to offer a method to avoid undesirable Li metal plating on the graphite anode during charging, and leads to a much longer battery lifetime and good charge capacity, all despite rapid charging.

## 1. Introduction

Electric vehicles (EVs) require a long-sought combination of large capacity, long life, and fast charging for them to be a compelling alternative to internal combustion vehicles. The U.S. Department of Energy devised the eXtreme Fast Charging (XFC) program,<sup>[1,2]</sup> supporting research and development from charging

A. Huang, J. Friend  
Materials Science and Engineering Program and the Department of  
Mechanical and Aerospace Engineering  
University of California San Diego  
9500 Gilman Drive, La Jolla, CA 92093, USA  
E-mail: jfriend@ucsd.edu

H. Liu, P. Liu  
Materials Science and Engineering Program and the Department of  
Nanoengineering  
University of California San Diego  
9500 Gilman Drive, La Jolla, CA 92093, USA  
E-mail: pliu@eng.ucsd.edu

The ORCID identification number(s) for the author(s) of this article can be found under <https://doi.org/10.1002/aesr.202200112>.

© 2022 The Authors. Advanced Energy and Sustainability Research published by Wiley-VCH GmbH. This is an open access article under the terms of the Creative Commons Attribution License, which permits use, distribution and reproduction in any medium, provided the original work is properly cited.

DOI: 10.1002/aesr.202200112

infrastructure,<sup>[3–6]</sup> the design of EVs,<sup>[2,7]</sup> battery packs,<sup>[8,9]</sup> and the content of the batteries themselves.<sup>[10–14]</sup> They established aggressive goals for improving LIB technology, seeking to deliver batteries that charge from zero to full capacity in 15 min with an energy density of 200 Wh kg<sup>-1</sup> and less than 20% fade in capacity after 500 cycles. These goals, combined, are well beyond several major technical barriers that have existed for decades.<sup>[1]</sup>

Fast charging a LIB requires high current flow, associated with a significant increase of overpotential on the graphite anode, pushing the operating potential of the anode toward the Li-plating potentials.<sup>[15]</sup> This reduces the performance, life, and safety of the LIB, and leads to lithium metal plating on the graphite anode instead of intercalating into the graphite, with undesirable side reactions and risk of internal shorting of the cells that may grow into thermal runaway.<sup>[16]</sup> High-performance

cells tend to use thin-layer or nanoparticle-based electrodes of electrochemically active media to minimize the diffusion distance.<sup>[15]</sup> The electrolyte is likewise tailored to improve the ionic conductivity and transport. Ion transport in the electrolyte underpins the charging speed of the LIB. Furthermore, the capacity of a LIB is limited by the ohmic potential across the electrolyte as the cutoff voltage is prematurely achieved during charging. Fast charging depletes the Li ions adjacent to the anode as their diffusion from the cathode and through the electrolyte via the separator is too slow to keep up, leading to a pronounced Li-ion concentration gradient, heating, and inhomogeneous Li deposition and plating.<sup>[17]</sup>

A major barrier to fast charging is the ionic conductivity of the electrolyte. A typical carbonate electrolyte in LIBs is LiPF<sub>6</sub> in ethylene carbonate (EC):dimethyl carbonate (DMC) at a weight ratio of 3:7 w w<sup>-1</sup>, with an ionic conductivity of 8.5 mS cm<sup>-1</sup> with 1 M LiPF<sub>6</sub> salt, which is sufficient for low charge rates of 0.1–1C. However, at high charge rates, > 3C, at least 13 mS cm<sup>-1</sup> is necessary to avoid undesirable chemical reactions.<sup>[18,19]</sup> Adding aliphatic esters—for example, methyl acetate (MA) or ethyl acetate (EA)—improves the ionic conductivity and overcomes this barrier while introducing another: decreasing the cycle life of the LIB through the formation of an undesirable solid electrolyte interphase (SEI) layer on the graphite anode.<sup>[20,21]</sup> Formate, nitriles, and amides have also been considered,<sup>[19]</sup> but poor compatibility with the LIB's cell chemistry reduces the Coulombic efficiency.<sup>[19]</sup> Notably, fluoroethylene carbonate

additive avoids these drawbacks, yet has one of its own: it is prone to defluorination by  $\text{PF}_5$  produced from the  $\text{LiPF}_6$  in the electrolyte.<sup>[22]</sup>

Beyond chemistry, other methods to increase the charge rate have been attempted. Exposure of the cathode to white light produces additional  $\text{Mn}^{4+}$  oxidation sites, improving charge transport.<sup>[23]</sup> External magnetic fields have been applied to produce electrolyte flow via magnetohydrodynamics:<sup>[24,25]</sup> a Lorentz force on the ions in the fluid electrolyte produces spiral-like flow, improving ion convection and helping to overcome the concentration gradient during fast charging. Unfortunately, magnetohydrodynamics is extraordinarily inefficient.<sup>[26]</sup>

Acoustic waves have been used as well, though mainly for sensing. Ladpli et al.<sup>[27]</sup> pioneered the use of pulsed ultrasound (US) transmission and detection to detect pouch cell degradation between the electrodes. Hao et al.<sup>[28]</sup> and Gold et al.<sup>[29]</sup> used a small piezoelectric transducer mounted on the outside for this purpose, employing instead a modulated sine wave to detect porosity and other morphological problems within the battery. Bommier et al.<sup>[30]</sup> used pulsed 2.25 MHz US to detect lithium plating on the graphite anode.

So far, the sole study on using acoustics as an actuator to enhance charging performance in batteries was the use of 100 MHz surface acoustic waves (SAW) in prototype lithium metal batteries.<sup>[31]</sup> Since that publication, there has been some work to more thoroughly explore the underpinning phenomena.<sup>[32]</sup> In other contexts, high-frequency US at 10–1000 MHz has been used to generate fluid and particle flow in micro to nanoscale confined structures somewhat analogous to the internal structure of batteries.<sup>[33,34]</sup>

We now integrate a SAW device into multilayer, nominally 1.8 Ah Li-ion pouch cells. These cells are made using standard graphite anodes,  $\text{LiNi}_{0.5}\text{Mn}_{0.3}\text{Co}_{0.2}\text{O}_2$  (NMC532) cathodes, and EC:DMC at 3:7 w w<sup>-1</sup> as our electrolyte. This carbonate electrolyte is widely known to be a poor choice for fast charging, and if a battery using this carbonate electrolyte can be shown to have good performance with fast charging, it may indicate other rechargeable batteries can benefit from the same technique.<sup>[18]</sup> Using SAW in this cell, we demonstrate the ability to avoid Li plating during fast (6C or 10 min) charging with SAW through electrochemical measurements, examination of the morphology via scanning electron microscopy (SEM), X-ray diffraction (XRD), energy-dispersive X-ray spectroscopy (EDX), and visual inspection of the LIB's components after disassembly. We further examine the LIB without disassembly using neutron diffraction. Throughout, we use pristine uncycled and no-SAW LIBs as controls. Altogether, integrated SAW appears to be an effective method to overcome the many barriers to fast LIB charging.

## 2. Experimental Section

### 2.1. Cell and SAW Device Fabrication

Pouch cells were chosen due to their manufacturing flexibility in commercial production.<sup>[35]</sup> The 1.8 Ah LIB pouch cells were composed of lithium nickel manganese cobalt oxide (NMC532) for the cathode and graphite for the anode. Specifically, the cathode was  $\text{LiNi}_{0.5}\text{Mn}_{0.3}\text{Co}_{0.2}\text{O}_2$  (NMC532): carbon nanotube (CNT):

polyvinylidene difluoride (PVDF) = 100:1:1.5 (Hong Xiang Battery Manufacturer, Yiyang City, Hunan Province, China) with a mass loading of 18.1 mg cm<sup>-2</sup>. The anode was a combination of carbon-based media, specifically carbon (C): carboxymethyl cellulose (CMC): styrene-butadiene rubber (SBR): superP conductive carbon black = 100:1.25:3:2 (Hong Xiang Battery Manufacturer, Yiyang City, Hunan Province, China), with a mass loading of 8.75 mg cm<sup>-2</sup>. To achieve consistent performance from individual 1.8 Ah pouch cells, the dry cell manufacture was outsourced to a commercial provider (Hong Xiang Battery Manufacturer, Yiyang City, Hunan Province, China). A commercial grade 1M solution of lithium hexafluorophosphate ( $\text{LiPF}_6$ ) in a 3:7 (w w<sup>-1</sup>) mixture of ethylene carbonate (EC) and dimethyl carbonate (DMC) (BASF, Ludwigshafen, Germany) was used as the electrolyte.

A 40 MHz SAW device was chosen and fabricated through lift-off lithography<sup>[36]</sup> to deposit 28 pairs of unweighted Au/Cr fingers and form an optimal<sup>[34]</sup> interdigital transducer (IDT) onto a 500  $\mu\text{m}$  thick 127.68° Y-rotated, X-propagating cut lithium niobate substrate ( $\text{LiNbO}_3$  (LN), University Wafer, Boston, MA, USA).<sup>[33,37]</sup> The process to choose the appropriate frequency and power for the SAW device based on the battery's dimensions and characteristics was described in the previous publication.<sup>[31]</sup> The SAW device was then coated with parylene C using chemical vapor deposition (PDS 2010 Parylene Coater System, Specialty Coating Systems, Indianapolis, IN, USA) to prevent reactions with the electrolyte<sup>[31]</sup> before introducing it into the bottom of the pouch LIB as shown in **Figure 1**. Electrolyte was first injected into the LIB with or without the SAW device inside an argon-filled glovebox (MTI Corporation), followed by de-gassing and final sealing (MTI Corporation, Richmond, CA). The moisture level and  $\text{O}_2$  level were both < 1 ppm. During experiments, the SAW device was operated with 100 mW input power only during charging.

### 2.2. Electrochemical Measurement

Electrochemical studies were carried out using the 1.8 Ah pouch LIB. For those LIBs with a SAW device, it was introduced at one end within the pouch, the SAW-carrying surface oriented toward the wrapped electrode-separator structure and perpendicular to the electrode gaps. The batteries were tested with battery cyclers (BST8-5A-CST and BST8-30A-CDS, MTI Corporation). The battery was first run through a formation cycle in a constant current (CC) mode, adopting constant current at a 0.1C charge rate to 4 V, followed by discharging at 0.1–2.5 V. After the formation cycle, the cells were then degassed in a glovebox with a vacuum sealer (MSK-115A, MTI Corporation) and resealed for further testing. From the second cycle, the battery was charged and discharged in a constant current (CC) mode; additional conditions specific to each experiment are individually defined in the article.

### 2.3. Morphological Characterization

After cycling, the batteries were disassembled inside an argon-filled glovebox to first observe their components' morphology via optical imaging. Representative areas were then cut out for SEM and EDX analysis (Quanta 250, FEI Corporation,

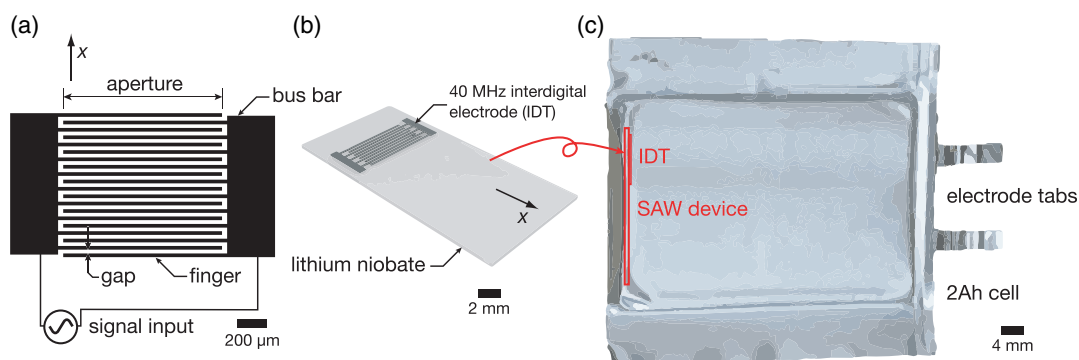


**Figure 1.** Introducing surface acoustic waves (SAW) into a 1.8 Ah pouch battery. a) The interdigital electrode (IDT) is defined by its aperture and finger and gap widths in this simple, straight IDT configuration. The IDT is plated upon: b) a lithium niobate substrate to produce a SAW device. Parylene coating the result before c) introducing it into a 1.8 Ah pouch cell and connecting it to a signal source protects it from damage from the electrolyte.

Hillsboro, OR). After rinsing with dimethyl carbonate (Sigma-Aldrich) to remove residual electrolyte, the electrodes were attached to a specimen holder (Ted Pella, Redding, CA) using double-side carbon tape (Ted Pella) and sealed within an aluminized polyethylene bag inside the glovebox. After transport to the SEM, the samples were quickly transferred from the bag to the SEM for imaging at 10 kV for the electrode material and 5 kV for the separators. The samples were exposed to air for less than three seconds to avoid air contamination.

#### 2.4. Crystallinity Characterization

The structural properties of the samples were characterized by XRD (Bruker D2 Phaser, Billerica, Massachusetts, USA) with a Cu  $\alpha$  radiation ( $\lambda = 1.5406 \text{ \AA}$ , 30 kV, 10 mA). The XRD results were collected in the range  $10^\circ < \theta < 80^\circ$  with a step size of  $2\theta = 0.02^\circ \text{ s}^{-1}$  to generate the best scanned intensity by removing the background noise. The electrodes were scratched off from the current collector, producing 0.3 g samples that were collected for each condition. The powder samples were then loaded into circular sample holders and sealed with polyimide tape (KAPTON HN966, DuPont de Nemours, Wilmington, DE USA) to prevent air contamination.

Neutron diffraction was employed to analyze, without disassembly, post-cycled batteries after 250 cycles using a 10 min charge time and 3 h discharge time for each cycle. The neutron diffraction was performed at the Spallation Neutron Source (SNS) at the Oak Ridge National Laboratory (ORNL, Oak Ridge, TN).<sup>[38]</sup> The time-of-flight (TOF) powder neutron diffraction data were collected on the VULCAN beamline (BL-7). The pouch cell was exposed to an incident, room-temperature neutron beam (5 mm by 5 mm) of 0.7–3.5  $\text{\AA}$  bandwidth, producing 0.5–2.5  $\text{\AA}$  d-space in the diffracted pattern of the  $\pm 90^\circ$   $2\theta$  detector banks, selected using double-disk choppers operating at 30 Hz. A high-intensity mode was employed with  $\Delta d/d 0.4\%$ <sup>[38]</sup> to collect powder neutron diffraction data for a duration of 0.5 h and processed using VDRIVE software.<sup>[39]</sup> Full pattern Rietveld refinement was performed using GSAS software with the EXPGUI interface.<sup>[40,41]</sup>

### 3. Results

#### 3.1. Cycling Performance

We first sought to determine the performance of the battery with and without SAW through its electrochemistry during cycling (Figure 2). We employed a range of charge and discharge currents, from a low current of C/18 (18 h charge and 18 h discharge) to an extremely high current of 6C (equivalent to a 10 min charge and a 10 min discharge) using independent, freshly prepared batteries after the formation cycle, degassing, and resealing. For the LIB with SAW, the SAW was only used during charging. At low current, the capacity is similar with or without SAW: both versions offer about 1.8 Ah. However, a difference becomes apparent as the charging current increases. As the charge rate is increased, the capacity of the LIB with or without SAW declines (Figure 2a). Using SAW improves the charge capacity retained by the battery above 1C. At 4C without SAW, the cell exhibits only 0.62 Ah of charge capacity, 37% of the C/18 capacity, and significantly less than the SAW-driven LIB (Figure 2b). By activating SAW in the LIB at 4C, the battery retains 1.06 Ah of capacity, 58% of the C/18 charged LIB (Figure 2c). For the first cycle at 6C, the SAW LIB offers 0.89 Ah, 78% more than the 0.50 Ah of the LIB without SAW. Presented as voltage versus capacity plots during the charge–discharge cycle, it is apparent that the absence of SAW (Figure 2b) reduces the battery's performance compared to the use of SAW (Figure 2c) as the charging rate is increased.

Perhaps the most illuminating result is the galvanostatic mode cycle at 6C (equivalent to a 10 min charge and a 10 min discharge) without SAW and the other with SAW during charging only, over a large number of cycles (Figure 2d). The cut-off voltages were defined to be 2.5–4.3 V. Without SAW, the capacity of the 1.8 Ah LIB was initially only 0.42 Ah due to the fast 6C charging, representing 100% capacity retention for that battery in this plot. Continuing cycling caused the no-SAW LIB to quickly lose its charge capacity—to less than 10% in fewer than 50 cycles. By 200 cycles, the no-SAW LIB had essentially no charge capacity, and the experiment was terminated for this battery at this point.

With SAW, 0.87 Ah capacity was obtained after one cycle, again representing 100% capacity retention in this plot. After

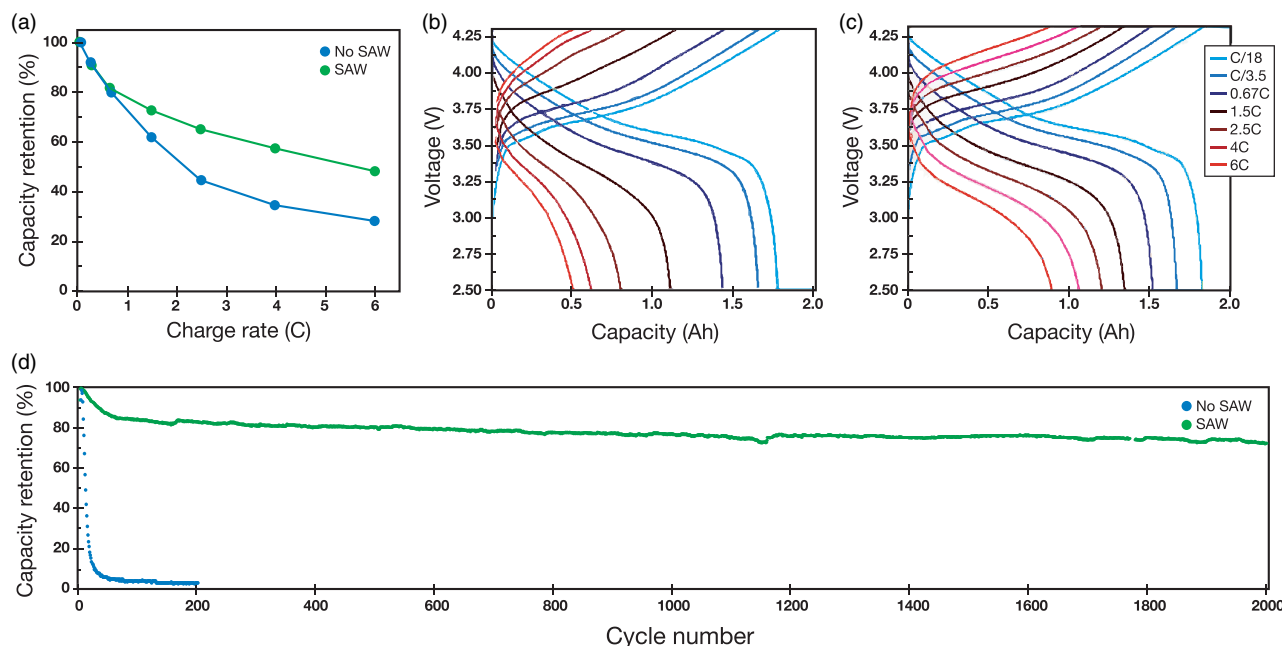


**Figure 2.** Electrochemical performance of a 1.8 Ah pouch lithium-ion battery (LIB) with and without SAW during charge–discharge cycling. a) The capacity retention after the first charge–discharge cycle of a LIB is plotted with respect to the charge rate used for that first cycle, 100 MHz SAW (SAW operating at 200 mW only during charging). It shows a progressive separation in the capacity as the charge and discharge currents were increased from C/18, C/3.5, 0.67C, 1.5C, 2.5C, and 4C to 6C. The corresponding voltage–capacity profiles for: b) the LIB without SAW shows greater polarization than the c) LIB using SAW. d) Long-term cycling performance of LIBs with and without SAW. Both cells were cycled in a galvanostatic mode with a 6C charge and C/3 discharge rate. Without SAW, the LIB's charge capacity was less than 10% before 50 cycles, and was essentially zero at 200 cycles. By comparison, with SAW, the LIB retained 80% of its initial capacity after 500 cycles and 72% of its initial capacity after 2000 cycles. The cut-off voltages were 2.5–4.3 V throughout.

50 cycles, the capacity of the LIB with SAW declined to 0.76 Ah, 87.4% of its initial capacity. Unlike the no-SAW LIB, the SAW LIB retained 80% of its initial capacity beyond 500 cycles, and stabilized at  $\approx 0.7$  Ah capacity thereafter. After 2000 cycles, the LIB still retained 72.5% of its initial capacity.

### 3.2. Neutron Diffraction

We next sought to determine the reasons for the observed improvement in LIB performance from SAW. We cycled a pair of LIB for 300 cycles with a fast 6C (10 min) charge and C/3 (3 h) discharge, the discharge time chosen in recognition of the typical EV application of these batteries. One LIB was operated with SAW during charging and the other without, after which the batteries were examined intact after complete discharge with neutron diffraction at ten locations as illustrated in **Figure 3a–c**. An uncycled pristine LIB was used for comparison. For reference, the SAW device was located on the right side of the pouch in **Figure 3c**, nearest points 5 and 10, and farthest from points 1 and 6. In the pristine LIB, the (110) and (108) peaks from the cathode are distinct and prominent at  $d = 1.435 \pm 0.01$  Å and  $1.447 \pm 0.08$  Å, respectively (**Figure 3d**). These two peaks are significantly shifted and broadened (**Figure 3e**) in the LIB without SAW after cycling to  $1.406$ – $1.437$  Å and  $1.436$ – $1.465$  Å, respectively. This result is correlated to the degradation of the battery's condition.

By comparison, the neutron diffraction peak distribution in the SAW LIB is less affected by cycling (**Figure 3f**). The peak signals have shifted, with the (110) peak shifting down to  $1.425 \pm 0.01$  Å and the (108) peak up to  $1.453 \pm 0.01$  Å. They are less homogeneously distributed compared to the pristine version. However, the peaks remain in a much narrower range compared to the cell cycled without SAW. This result suggests that SAW during charging reduces the degradation of the LIB's materials.<sup>[42]</sup>

We also consider the lattice constants  $a$  and  $c$  for the cathode and anode as plotted in **Figure 3g–m**. For the (g) cathode, the  $c$  lattice constants for the pristine battery at different locations are consistent, and the average value is  $14.2322$  Å with a maximum of  $14.2341$  Å and a minimum of  $14.2304$  Å. For the SAW-absent LIB and SAW-driven LIB, the average value of the  $c$  lattice constant is  $14.4307$  Å and  $14.36015$  Å, respectively. The average  $c$  lattice constant of NMC cathode materials in the battery with SAW indicates less Li remains in the cathode, caused by irreversible Li loss during battery cycling.<sup>[43]</sup> The smaller  $c$  lattice constant for the SAW-driven battery's cathode is an indicator of its better cycling performance and higher reversible cell capacity. Moreover, the consistent cathode's  $c$  lattice constant across the different locations in the battery indicates that the electrochemical reactions within are more spatially homogeneous with SAW. This is especially clear when comparing the range of the  $c$  lattice constant of the SAW-driven battery's cathode,  $0.0344$  Å, to the cathode of the battery without SAW,  $0.1184$  Å: the latter is 3.4

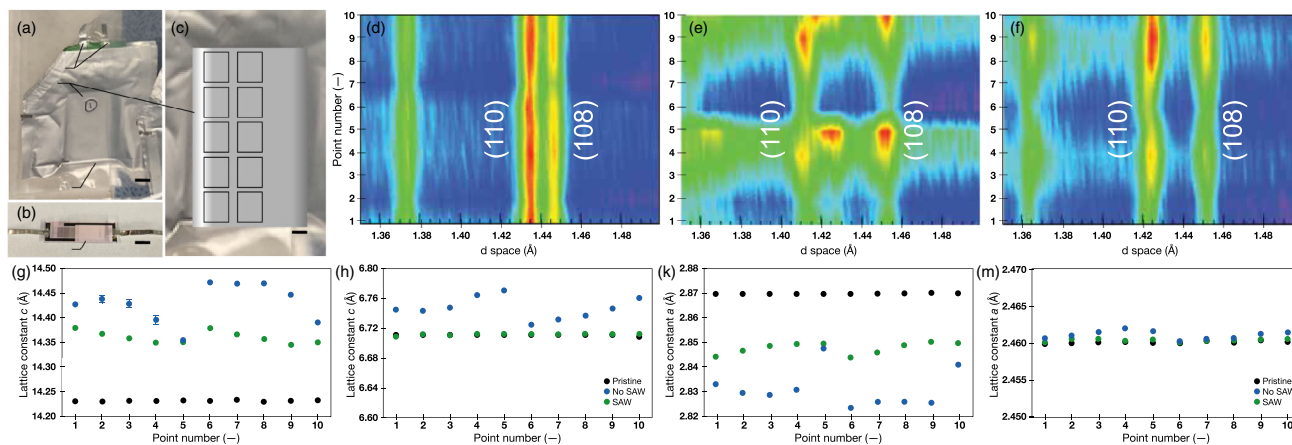


**Figure 3.** Neutron diffraction results of the LIB at a pristine stage, after cycling without SAW, and after cycling with SAW. a) The pouch LIB with battery connection tabs at the top and the SAW device, hidden within the pouch, at the bottom. The tabs to connect to the: b) SAW device protrude (a) from the sides of the pouch in this prototype. For neutron diffraction, c) ten points were defined on the battery, with points 1–5 adjacent to the left edge and 6–10 down the centerline of the battery. Points 1 and 6 are closest to the battery tabs and farthest away from the SAW device, while points 5 and 10 are closest to the SAW device at the bottom. d–f) The diffraction results for (d) a pristine, uncycled LIB across points 1–10 indicate an initially well-defined structure. After 300 cycles without SAW, the (e) neutron diffraction shows substantial broadening and shifting of the diffraction. By contrast, the LIB cycled with SAW (f) shows some peak shifting but more limited broadening. The changes in the lattice constants: g,h)  $c$  and k,m)  $a$  of the LIB from (black) pristine to (blue) with SAW and (red) without SAW are provided for the (g,k) cathode and (h,m) anode for the (c) ten measurement points on the LIB.

times larger. In any case, the difference is significant based on a Student's  $t$ -test of the results (Shapiro-Wilk indicates a normal distribution;  $p = 1.89 \times 10^{-4}$ ).

In contrast, the  $a$  lattice constant (Figure 3k) decreases from 2.8697 Å to 2.8308 Å without SAW and 2.8475% with SAW. The reduction in  $a$  from cycling is 1.36% in the LIB without SAW and 0.77% with SAW, respectively. The  $a$  lattice constant shrinks when Li is extracted from the NMC cathode material. The smaller  $a$  lattice constant of cathode materials in the battery with SAW confirms Li loss during battery cycling. However, there is no significant difference in the  $a$  lattice constant between the no-SAW and with-SAW conditions (Shapiro-Wilk indicates not normally distributed; Wilcoxon rank sum test produces  $p = 0.7045 \gg 0.05$  rejecting significance).

The lattice constants for the anode vary far less from cycling, but still produce a significant difference depending on whether or not SAW is used during the charging of the LIB. The pristine graphite anode has a  $c$  lattice constant (Figure 3h) of 6.7114 Å that increases to 6.7479 Å and 6.7124 Å, respectively, for a cycled LIB without SAW and with SAW. This represents an average 0.54% increase in  $c$  without SAW from the pristine state, much more than the 0.01% increase with SAW. The  $a$  lattice constant slightly increases from 2.4601 Å for the pristine LIB to 2.4612 Å and 2.4605 Å after cycling without and with SAW, respectively. The change in  $a$  is 0.05% without SAW and 0.02% with SAW, small but significantly different, as judged via the Wilcoxon rank-sum test ( $p = 0.0012 < 0.05$ ). This test was used as the observed results here were weakly non-parametric according to a Shapiro-Wilk test. Combining these lattice constant changes for the cathode, it is apparent the Li loss is greater in the cycled LIB without SAW, and that the degradation of the cathode is reduced using SAW during fast charging. At the same time, the improvement in the spatial uniformity of the electrochemical

reactions inside the battery via the SAW under fast charging conditions is confirmed.

### 3.3. Ex situ Characterization of the Material from Cycled Cells

Visual inspection of a disassembled LIB after cycling shows significantly more deposition in a LIB after 200 cycles without SAW than in a LIB after 2000 cycles with SAW. This concurs with the electrochemical performance observations provided in Figure 2: after 200 cycles, the no-SAW LIB has essentially zero capacity while the SAW-driven LIB still reports 72% of its initial capacity after 2000 cycles. There is little apparent difference in the cathode (Figure 4a) between the two batteries, with the differences remaining visually inconspicuous. However, the surface of the separator facing the cathode after 200 cycles has ample metallic-brown deposits in the LIB without SAW. These deposits are largely absent in the SAW LIB even after 2000 cycles. This discrepancy is also apparent on the anode, with ample metallic deposits on the LIB without SAW but only a few small regions of the SAW LIB anode. The anode-facing side of the separator also shows a substantial difference between the two batteries, with over 90% of the exposed separator covered by these deposits on the no-SAW LIB that are, again, absent on the separator from the SAW LIB.

A closer look at the anode surfaces, in particular using SEM, shows a rougher, dendritic morphology in the LIB without SAW (Figure 5a,b), with porous  $\approx 2 \mu\text{m}$  grains forming an uneven, cracked morphology of  $\approx 100 \mu\text{m}$  order. The surface structure appears to be plated Li and side products from the reaction of Li with the electrolyte,<sup>[44]</sup> typical of fast-charging LIBs without an effective strategy to avoid Li plating. The anode of the SAW LIB (Figure 5c–d) is comparatively smooth and composed

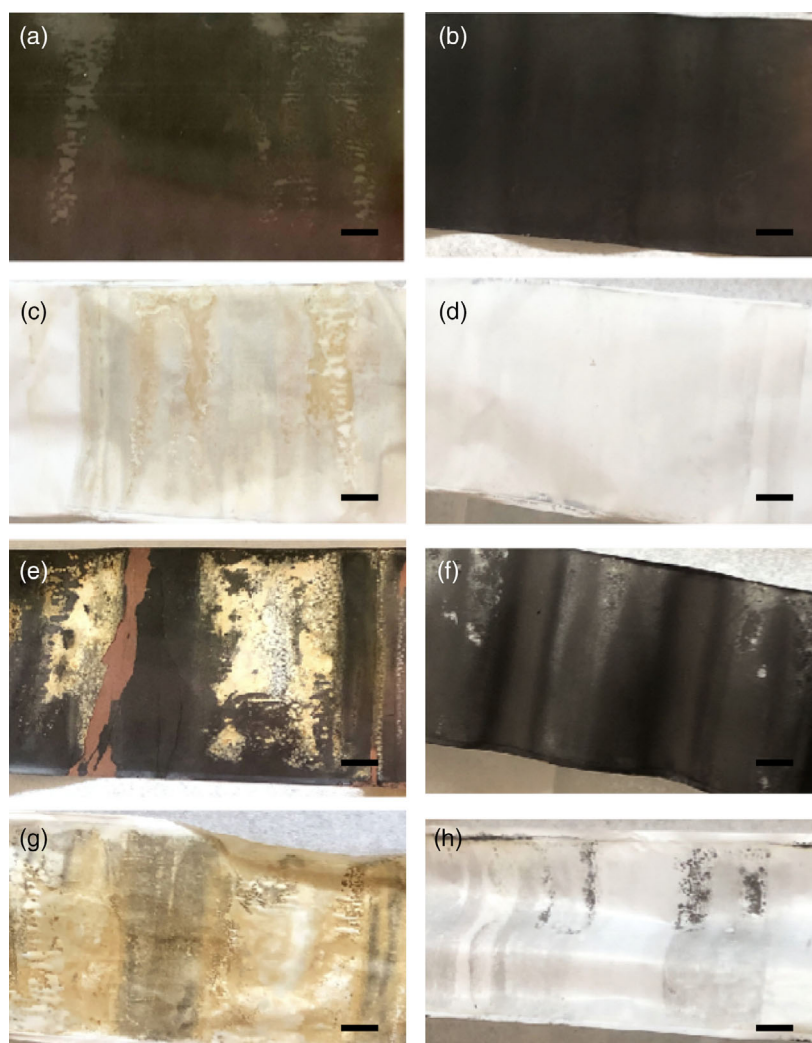


**Figure 4.** Visible surface morphology of the components within cycled LIB cells with and without SAW. The a,c,e,g) left column presents the components of the no-SAW LIB after 200 6C charge and C/3 discharge cycles, while the b,d,f,h) right column presents the components of the SAW LIB after 2000 6C charge and C/3 discharge cycles. By row, the images show: a,b) the cathode, c,d) the cathode side of the separator, e,f) the anode, and g,h) the anode side of the separator. There are evident deposits on the electrodes and separator for the no-SAW battery components; these are largely absent on the LIB with SAW. All scale bars are 10 mm.

of chunked particles at  $\approx 10 \mu\text{m}$  representative of pristine graphite,<sup>[44]</sup> regardless of the imaging position in Figure 5c,d.

Moreover, the SAW LIB appears to have a thinner SEI formation than the LIB without SAW. Notwithstanding the typical drawbacks of EDX, especially its inability to resolve Li, the ratio of C:F:O with SAW after 2000 cycles was 1:0.16:0.11 compared to 1:0.31:0.21 without SAW after 200 cycles in the protocol reported in this subsection. The reduced fractions of fluoride and oxygen suggest the degradation of the electrolyte and anode are reduced when using SAW, because they represent typical SEI components.<sup>[45]</sup>

Similar effects are present in the separator. For the anode side of the separator (Figure S1, Supporting Information), whisker-like Li dendrite morphology was found on the surface after cycling the cell without SAW (Figure S1a,b, Supporting Information). However, the separator remained smooth after cycling the battery with SAW, regardless of the position that

was imaged with respect to the SAW device's location (Figure S1c,d, Supporting Information, are images closer to the SAW device, at point 10 in Figure 3c, while Figure S1e,f, Supporting Information, are further away, at point 6 in Figure 3c). For the cathode side of the separator, the morphology change was less obvious, similar to the less obvious changes observed in the cathode itself. However, it was still found that more deposition was present on the separator's surface after cycling 200 times without SAW (Figure S2a,b, Supporting Information) compared to the separator's surface after 2000 cycles with SAW (Figure S2c,d, Supporting Information).

### 3.4. Material Characterization of the Electrodes

Turning next to XRD, we compared the anodes and cathodes of a pristine LIB to a LIB cycled without SAW after 200 cycles and a

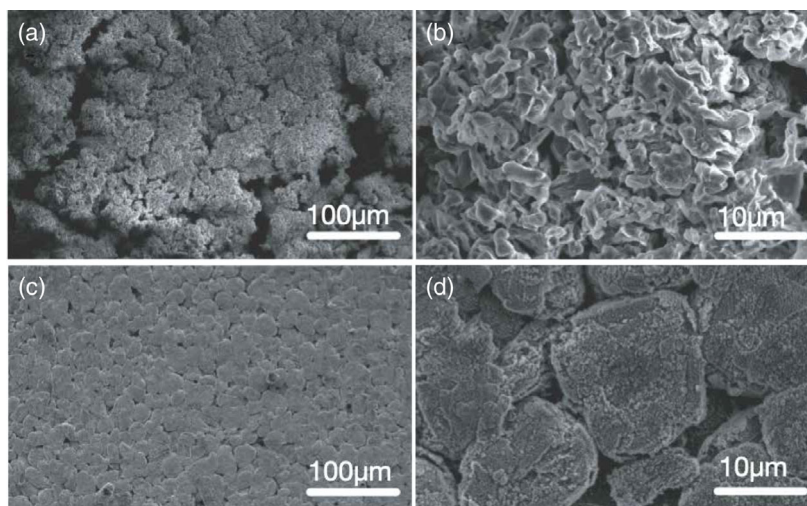


**Figure 5.** Scanning electron microscopy (SEM) images of the cycled LIB anodes. a) After 200 cycles, a porous, cracked, and dendritic morphology is present upon the anode surface, formed of: b)  $\approx 2 \mu\text{m}$  grains. After 2000 cycles with SAW, c,d) the anode morphology appears more uniform and dense, formed d of chunked particles resembling pristine graphite.

LIB cycled 2000 times with SAW, both cycled at 6C charge and C/3 discharge rates, and all in Figure 5. The representative peak<sup>[46]</sup> for the anode's graphite is present at  $26.82^\circ$  in **Figure 6a** for the pristine anode, marked with an asterisk (\*) in the plot.

Measurements using XRD were performed on the LIB without SAW at two locations, one in a region without the metallic deposition (black), and another with it (metallic). The XRD reveals a peak shifted ( $\dagger$  in Figure 6a) from  $26.82^\circ$  to a lower scattering angle of  $25.38^\circ$ , correlated to a lithiated  $\text{LiC}_x$  ( $\text{LiC}_{12}$ ,  $\text{LiC}_{24}$ , for example) graphite phase formation.<sup>[30,46]</sup>

From a region with metallic deposits, the  $26.82^\circ$  peak is smaller, overwhelmed by a broader peak at  $25.67^\circ$  and indicative of a new  $\text{LiC}_x$  crystalline phase.<sup>[30]</sup> The observation of the lithiated graphite phase indicates some Li is trapped in the graphite, causing an inhomogeneous capacity degradation across the cell.

With SAW, the anode's XRD peaks remain narrow and strong, though slightly shifted to  $26.67^\circ$  and  $26.81^\circ$  from the original  $26.82^\circ$ , respectively, for points near and far from the SAW device. The near point is point 10 in Figure 3c) and the far point is point 6 in Figure 3c. This indicates that 2000 cycles at 6C charging do not degrade the graphite anode in the LIB with SAW.

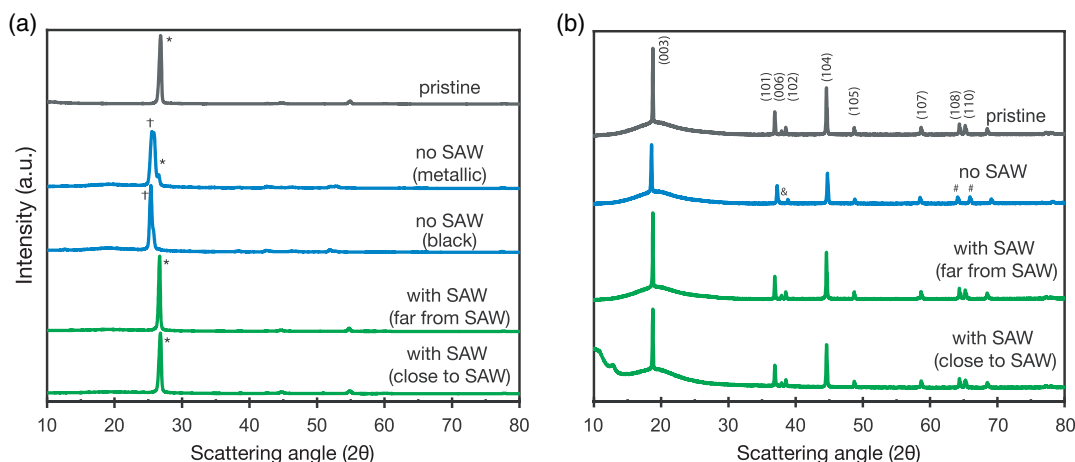


**Figure 6.** X-ray diffraction (XRD) of the anodes and cathodes of a LIB with and without SAW. a) XRD of anodes taken from a LIB immediately after the formation cycle is shown as a pristine result (gray line). This is compared to the XRD at two points of the anode from a LIB cycled at 6C charge and C/3 discharge rates for 200 cycles without SAW (blue lines). Referring to Figure 4e, the two “no SAW” results are taken from a point with metallic deposits, “metallic,” and a point where there were no such deposits, “black.” The XRD of two points on the anode (green lines)—near (at point 10 in Figure 3c) and far away (at point 6 in Figure 3c) from the SAW device—in a LIB with SAW cycled 2000 times at 6C charge and C/3 discharge rates complete this plot. The \* represents the graphite phase, while  $\dagger$  represents the  $\text{LiC}_{12}$  (for example,  $\text{LiC}_{24}$  or  $\text{LiC}_{24}$ ) phase. b) The XRD of the cathode is similar, with only one no-SAW result shown as there are no metallic deposits upon the cathode. The & represents the missing (006) phase from the no-SAW LIB, while # shows the large separation in the angular position of the peaks between the (108) and (110) phases in the no-SAW LIB's cathode.

The corresponding measurement of the cathode in Figure 6b show broadly similar results from the pristine and cycled versions of the LIB with SAW. The pristine NMC 532 shows a hexagonal layered structure with an R3m space group and phases that appear to match past literature.<sup>[47]</sup> A closer look is illuminating, however, with peaks at (003), (104), (101), (006), and (102) remaining at the same angles and with similar widths for all versions of the LIB—except for the battery cycled without SAW. In the no-SAW LIB, the peaks associated with the (003), (006) (note &), (108), and (110) (note # symbols) axes have shifted or disappeared, indicating a change in the cathode's lattice structure with strain and material degradation.<sup>[42]</sup> It is worth noting that the separation of peaks (108) and (110)(note # symbols) of the cathode material is evident in the no-SAW LIB, indicating a large change in the cathode's lattice structure with strain and material degradation.<sup>[42]</sup> By comparison, the SAW LIB's cathode XRD results appear similar to the pristine LIB cathode, even after 2000 cycles. The qualitative results from XRD are consistent with the quantitative lattice parameter analysis from the neutron diffraction, indicating that SAW is beneficial to the battery's cycling.

#### 4. Discussion

Without SAW-driven acoustic streaming to cause electrolyte recirculation in the LIB, the Li ions are drawn from the electrolyte and intercalated into the graphite anode of the LIB only if the electrical current is low enough to allow diffusion to occur. The SAW itself generates laminar flow from acoustic streaming within the battery structure. Details of this mechanism, including a model and representative design concepts, are provided in our past work,<sup>[31]</sup> though there are distinct differences in the mechanism at play in LIBs. Some discussion of the cost of SAW devices is perhaps appropriate here, though any cost prediction strongly depends on volume, construction, and similar factors that are impossible to estimate until the work transitions from research to development and onwards to production.<sup>[48]</sup> In our analysis, based on discussions with possible SAW device manufacturers, 2.4 MWh of batteries, about 266 000 cells, would each cost ten cents more, increasing their unit cost by about 8%. A larger run of 2.4 GWh of batteries, or 266M cells, would each cost one cent more. However, because it is possible to at least double the cycle life of the battery, the overall cost per cycle-kWh is reduced by more than 50% compared to current LIBs. The cost is further reduced when taking into account the ability to reduce the charging time and therefore improve the use of charging infrastructure, a key bottleneck in EVs.

At the fast charge rates needed for EVs and other applications, when the Li-ion diffusion rate is insufficient, a high overpotential exists on both the cathode and the anode. From the large cell polarization, the battery will reach its cut-off voltage at a lower state of charge, delivering a lower charge and discharge capacity. As shown in Figure 2b,c, the battery without SAW presented an elevated cell voltage at a 6C charge rate compared to the battery with SAW. With the same charge cut-off voltage of 4.3 V, the cell without SAW delivers only 0.50 Ah capacity, while the cell with SAW delivers 0.89 Ah capacity. This proves that SAW helps to reduce the electrode overpotential via Li ion transport from induced electrolyte flow. The other issue is the risk of Li plating

on the graphite anode, introduced by the high overpotential on the anode that pushes the graphite operating potential to  $<0$  V versus Li<sup>+</sup>/Li. Visually, the metallic Li deposition is apparent upon the anode and the separator when cycling the battery without SAW at a 6 C rate (Figure S1, Supporting Information). The Li metal plating on the graphite is likely irreversible; it either reacts with the electrolyte to generate side products or forms electrochemically inactive Li. Apparently, SAW produces a positive effect in fast charging LIBs. Even after 2000 cycles, the metallic deposits were absent on the separator and anode. The result correlates with the electrochemical results in Figure 2, where the charge capacity for the battery that cycled without SAW rapidly declined. By contrast, 72% of the SAW-driven LIB's capacity was retained after 2000 cycles.

Often, there are questions regarding the true mechanism underlying SAW use in rechargeable batteries. Beyond the details of the mechanism and exploration of the relevant parameters provided in the context of recharging lithium batteries in the past,<sup>[31]</sup> we consider this question here. The power used by the SAW device during LIB charging is about 100 mW, applied for about 10 min with charging at 6C. The change in the LIB's temperature may be determined by using the relation between the temperature change,  $\Delta T$ , the input power,  $Q$ , and the heat capacity,  $c$ , and mass,  $m$ , of the battery:  $Q = mc\Delta T$ . To provide an estimate of the temperature change, we make the conservative assumption that all the acoustic energy input becomes heat, such that  $Q = (100 \text{ mW})(3600 \text{ s}) = 3.6 \times 10^2 \text{ J}$  is over our 10 min charge cycle. We furthermore conservatively estimate that the entire battery has a specific heat matching graphite,  $c = 0.79 \text{ J(g K)}^{-1}$ , noting that the electrolyte and metals will have a much greater specific heat that will act to reduce the temperature change. The mass of the 1.8 Ah battery is, finally,  $m = 70 \text{ g}$ , and so we find that  $\Delta T = 1 \text{ K}$ . In other words, under an especially conservative estimate, the temperature increase due to the use of SAW during charging is about one degree. In actual measurements of the temperature of the LIB during 6C charging with SAW, we found that the temperature of the battery actually decreased by 3 °C from 38 °C at the start of charging to 35 °C at the completion of charging. The likely mechanism is the reduction of the Li-ion depletion region adjacent to the anode due to SAW-induced flow. This effect can be observed in the electrochemical results: with SAW, the overpotential is lowered.

In rapid charging conditions, due to the slow mass transfer, the electrochemical reaction in the battery is nonuniform. Reexamining the neutron diffraction results (Figure 3), the (110) and (108) phases from the pristine LIB's cathode are distinct and prominent at  $d \approx 1.435 \pm 0.01 \text{ \AA}$  and  $1.475 \pm 0.08 \text{ \AA}$ , respectively, with another, a weaker signal at  $1.375 \text{ \AA}$ . These signals are significantly shifted and broadened (Figure 3e) after cycling, with (110) at  $1.406\text{--}1.437 \text{ \AA}$  and (108) at  $1.436\text{--}1.465 \text{ \AA}$ . Without SAW, the large variation of the cathode structure at different locations of the cell indicates the electrochemical reactions in the cell are spatially inhomogeneous. This inhomogeneity in the cell's degradation accelerates the overall cell degradation as the electrochemistry progressively diverges across the cell. With SAW, the (110) peak shifted down to  $1.425 \pm 0.01 \text{ \AA}$  and the (108) peak up to  $1.453 \pm 0.01 \text{ \AA}$ , but they largely remain intact and narrow, leading to spatially uniform reactions inside the battery and

maintaining good cycle performance. However, much more work is needed to determine the details of this mechanism. Our focus in this article has been to demonstrate the strong effect of SAW in fast charging LIBs.

## 5. Conclusions

By choosing a 1.8 Ah lithium-ion-based battery with an NMC532 cathode, a graphite anode, and a carbonate-based electrolyte (EC/DMC with 1M LiPF<sub>6</sub>), we sought in this study to explore the impact of using SAW in improving practical battery performance, especially for high-speed charging so desirable in EVs and other mobility solutions today and into the future. This method is chemistry agnostic, in that other battery chemistries could conceivably be used with SAW to improve their overall performance, especially with regard to expanding the range of charging speed, cycle lifetime, and capacity. The SAW devices themselves are durable and tolerate temperatures well outside the general design envelope of rechargeable batteries. In this study, we explored only using the SAW during charging to avoid lithium plating upon the anode as the most serious problem facing the application of LIBs to fast charging systems, though there may be merit in considering the use of SAW during especially rapid discharge—for example, during rapid acceleration of an EV—to overcome heating or damage.

Moreover, the SAW device was integrated into the pouch of the battery in this study to increase the amplitude of the transmitted acoustic wave upon the electrolyte present between the anode and cathode within the battery. It is reasonable to consider how to use acoustic devices, such as the SAW device outside instead of inside the pouch, or even outside a jellyroll or other types of LIB. Our very preliminary results indicate that, in doing so, the benefit of introducing the acoustic device is reduced but remains significant. There may well be an optimal configuration of an acoustic device and one or more batteries that would produce the greatest improvement in performance without requiring the retooling of the battery manufacturing facilities. One must keep in mind, of course, that introducing a new component into a battery brings additional complexity, though by virtue of its decades of use in telecommunications, the lithium niobate-based SAW device is at least a developed technology. Adapting it into battery manufacture requires thought and planning on ways to minimize acoustic energy loss from the device to the electrolyte. Some battery designs incorporate acoustically lossy materials such as plastics and foams that may need to be reconsidered to make the use of the SAW device work in this application.

Ideally, the charge capacity of our pouch LIB would be greater despite the very large charging speeds; a 50% reduction of the battery's baseline capacity from 1.8 Ah to 0.9 Ah by radically increasing the charging and discharging speed from C/18 to 6C is unfortunate in light of applications. However, we did not adopt any of the industry-standard techniques of CC-CV charging methods nor any battery management methods that are able to improve the capacity-charge rate result. Our main aim was to provide a simple and straightforward basis for comparison, demonstrating that by using SAW one could achieve a far longer battery lifetime despite the rapid charge and discharge rates. Regardless, it is apparent that by including SAW in a LIB it

becomes possible to charge and discharge the battery at very high speeds without adversely and permanently affecting its performance. By combining the SAW-based approach with advanced battery management, improved chemistry, and other techniques, it is likely that significant improvements in batteries relevant to EVs and related applications can be achieved.

## Supporting Information

Supporting Information is available from the Wiley Online Library or from the author.

## Acknowledgements

The authors are grateful for the support of this work by the Department of Energy via grant DE-EE0008363. The work presented here was furthermore generously supported by a research grant to J. Friend from the W.M. Keck Foundation. The authors are grateful to the University of California, the Qualcomm Institute, and the NANO3 facility at UC San Diego for the provision of funds and facilities in support of this work. This work was performed in part at the San Diego Nanotechnology Infrastructure (SDNI) of UCSD, a member of the National Nanotechnology Coordinated Infrastructure, which is supported by the National Science Foundation (Grant ECCS-1542148). A portion of this research used resources at the Spallation Neutron Source, a DOE Office of Science User Facility operated by the Oak Ridge National Laboratory. The authors thank Dr. Y. Chen and Dr. K. An at SNS for their support of neutron experiments.

## Conflict of Interest

A.H. and H.L. have started *Sonocharge*, a company based in part on the results provided in this article. P.L. and J.F. have equity in this company. This company was started after the completion of the research work reported in this article. Intellectual property protection has been filed with U.S. patent 11,196,092 issued on December 7, 2021, and Patent Cooperation Treaty Patent Application PCT Patent Application WO 2021/026043 A1 filed with a priority date of August 1, 2020.

## Data Availability Statement

The data that support the findings of this study are available from the corresponding author upon reasonable request.

## Keywords

acoustofluidics, fast charging, lithium ion batteries, ultrasound

Received: August 11, 2022

Revised: November 9, 2022

Published online:

- [1] S. Ahmed, I. Bloom, A. N. Jansen, T. Tanim, E. J. Dufek, A. Pesaran, A. Burnham, R. B. Carlson, F. Dias, K. Hardy, M. Keyser, *J. Power Sources* **2017**, 367, 250.
- [2] A. Masias, J. Marcicki, W. A. Paxton, *ACS Energy Lett.* **2021**, 6, 621.
- [3] H. Mehrjerdi, R. Hemmati, *J. Energy Storage* **2019**, 26, 100924.
- [4] J. Wenig, M. Sodenkamp, T. Staake, *Appl. Energy* **2019**, 255, 113787.
- [5] G. Alkaws, Y. Baashar, D. Abbas U, A. A. Alkahtani, S. K. Tiong, *Appl. Sci.* **2021**, 11, 3847.

- [6] B. Lebrouhi, Y. Khattari, B. Lamrani, M. Maaroufi, Y. Zeraouli, T. Kousksou, *J. Energy Storage* **2021**, *44*, 103273.
- [7] A. H. Akinlabi, D. Solyali, *Renewable Sustainable Energy Rev.* **2020**, *125*, 109815.
- [8] Y. Zheng, Y. Shi, Y. Huang, *Appl. Therm. Eng.* **2019**, *147*, 636.
- [9] X. Tan, P. Lyu, Y. Fan, J. Rao, K. Ouyang, *Appl. Therm. Eng.* **2021**, *196*, 117279.
- [10] S. S. Zhang, *InfoMat* **2021**, *3*, 125.
- [11] M. Weiss, R. Ruess, J. Kasnatscheew, Y. Levartovsky, N. R. Levy, P. Minnmann, L. Stolz, T. Waldmann, M. Wohlfahrt-Mehrens, D. Aurbach, M. Winter, *Adv. Energy Mater.* **2021**, *11*, 2101126.
- [12] S. Q. Li, K. Wang, G. F. Zhang, S. N. Li, Y. N. Xu, X. D. Zhang, X. Zhang, S. H. Zheng, X. Z. Sun, Y. W. Ma, *Adv. Funct. Mater.* **2022**, *32*, 2200796.
- [13] Y. Liu, Y. Zhu, Y. Cui, *Nat. Energy* **2019**, *4*, 540.
- [14] A. Tomaszewska, Z. Chu, X. Feng, S. O'Kane, X. Liu, J. Chen, C. Ji, E. Endler, R. Li, L. Liu, Y. Li, *ETransportation* **2019**, *1*, 100011.
- [15] A. M. Colclasure, T. R. Tanim, A. N. Jansen, S. E. Trask, A. R. Dunlop, B. J. Polzin, I. Bloom, D. Robertson, L. Flores, M. Evans, E. J. Dufek, *Electrochim. Acta* **2020**, *337*, 135854.
- [16] D. Lu, Y. Shao, T. Lozano, W. D. Bennett, G. L. Graff, B. Polzin, J. Zhang, M. H. Engelhard, N. T. Saenz, W. A. Henderson, P. Bhattacharya, *Adv. Energy Mater.* **2015**, *5*, 1400993.
- [17] X. Zhang, L. Zou, Y. Xu, X. Cao, M. H. Engelhard, B. E. Matthews, L. Zhong, H. Wu, H. Jia, X. Ren, P. Gao, *Adv. Energy Mater.* **2020**, *10*, 2000368.
- [18] E. Logan, J. Dahn, *Trends Chem.* **2020**, *2*, 354.
- [19] A. M. Haregewoin, A. S. Wotango, B.-J. Hwang, *Energy Environ. Sci.* **2016**, *9*, 1955.
- [20] R. Petibon, J. Harlow, D. Le, J. Dahn, *Electrochim. Acta* **2015**, *154*, 227.
- [21] X. Wu, T. Liu, Y. Bai, X. Feng, M. M. Rahman, C.-J. Sun, F. Lin, K. Zhao, Z. Du, *Electrochim. Acta* **2020**, *353*, 136453.
- [22] I. A. Shkrob, J. F. Wishart, D. P. Abraham, *J. Phys. Chem. C* **2015**, *119*, 14954.
- [23] A. Lee, M. Voros, W. M. Dose, J. Niklas, O. Poluektov, R. D. Schaller, H. Iddir, V. A. Maroni, E. Lee, B. Ingram, L. A. Curtiss, *Nat. Commun.* **2019**, *10*, 1.
- [24] K. Shen, X. Xu, Y. Tang, *Nano Energy* **2022**, *92*, 106703.
- [25] K. Shen, Z. Wang, X. Bi, Y. Ying, D. Zhang, C. Jin, G. Hou, H. Cao, L. Wu, G. Zheng, Y. Tang, *Adv. Energy Mater.* **2019**, *9*, 1900260.
- [26] S. Qian, H. H. Bau, *Mech. Res. Commun.* **2009**, *36*, 10.
- [27] P. Ladpli, F. Kopsaftopoulos, F.-K. Chang, *J. Power Sources* **2018**, *384*, 342.
- [28] W. Hao, Z. Yuan, D. Li, Z. Zhu, S. Jiang, *J. Energy Storage* **2021**, *41*, 102894.
- [29] L. Gold, T. Bach, W. Virsik, A. Schmitt, J. Muller, T. E. Staab, G. Sextl, *J. Power Sources* **2017**, *343*, 536.
- [30] C. Bommier, W. Chang, Y. Lu, J. Yeung, G. Davies, R. Mohr, M. Williams, D. Steingart, *Cell Rep. Phys. Sci.* **2020**, *1*, 100035.
- [31] A. Huang, H. Liu, O. Manor, P. Liu, J. Friend, *Adv. Mater.* **2020**, *32*, 1907516.
- [32] O. Dubrovski, O. Manor, *Phys. Rev. Mater.* **2021**, *5*, 123402.
- [33] J. Friend, L. Y. Yeo, *Physics* **2011**, *83*, 647.
- [34] W. Connacher, N. Zhang, A. Huang, J. Mei, S. Zhang, T. Gopesh, J. Friend, *Lab Chip* **2018**, *18*, 1952.
- [35] J. Liu, Z. Bao, Y. Cui, E. J. Dufek, J. B. Goodenough, P. Khalifah, Q. Li, B. Y. Liaw, P. Liu, A. Manthiram, Y. S. Meng, *Nat. Energy* **2019**, *4*, 180.
- [36] J. Mei, N. Zhang, J. Friend, *J. Visualized Exp.* **2020**, *160*, e61013.
- [37] A. Huang, M. Miansari, J. Friend, *Appl. Phys. Lett.* **2018**, *113*, 034103.
- [38] K. An, H. D. Skorpenske, A. D. Stoica, D. Ma, X.-L. Wang, E. Cakmak, *Trans. A* **2011**, *42*, 95.
- [39] X.-L. Wang, C. T. Liu, U. Keiderling, A. Stoica, L. Yang, M. K. Miller, C. L. Fu, D. Ma, K. An, *J. Alloys Compd.* **2012**, *529*, 96.
- [40] A. C. Larson, R. B. Von Dreele, *General Structure Analysis System (gsas)(report Laur 86-748)*, Los Alamos National Laboratory, Los Alamos, New Mexico **2004**.
- [41] B. H. Toby, *J. Appl. Crystallogr.* **2001**, *34*, 210.
- [42] A. O. Kondrakov, A. Schmidt, J. Xu, H. Geswein, R. Monig, P. Hartmann, H. Sommer, T. Brezesinski, J. Janek, *J. Phys. Chem. C* **2017**, *121*, 3286.
- [43] W. Li, H. Y. Asl, Q. Xie, A. Manthiram, *J. Am. Chem. Soc.* **2019**, *141*, 5097.
- [44] C. Fear, T. Adhikary, R. Carter, A. N. Mistry, C. T. Love, P. P. Mukherjee, *ACS Appl. Mater. Interfaces* **2020**, *12*, 30438.
- [45] N. L. Hamidah, F. M. Wang, G. Nugroho, *Surf. Interface Anal.* **2019**, *51*, 345.
- [46] D. Allart, M. Montaru, H. Gualous, *J. Electrochem. Soc.* **2018**, *165*, A380.
- [47] R. Weber, C. R. Fell, J. Dahn, S. Hy, *J. Electrochem. Soc.* **2017**, *164*, A2992.
- [48] R. Roy, S. Colmer, T. Griggs, *Int. J. Prod. Econ.* **2005**, *97*, 210.